Validation of a non-contact technique for torque measurements in wind turbines using an enhanced transient FSV approach

G. Zhang [a], D. Zappalá [b,*], C. Crabtree [b], C. Donaghy-Spargo [b], S. Hogg [b], A. Duffy [c]

[a] Harbin Institute of Technology, Harbin, China
[b] Department of Engineering, Durham University, South Road, Durham, UK
[c] School of Engineering and Technology, De Montfort University, Leicester, UK

ARTICLE INFO

ABSTRACT

In-service turbine monitoring is essential for maximizing the wind energy contribution to the global energy budget. Measurement of turbine shaft torque under transient wind conditions is fundamental to develop reliable condition monitoring techniques. Contact based measurements bring their own disadvantages and non-contactless measurements have many potential advantages. However, their performance needs to be validated against standard methods. This paper focuses on the development of an enhanced transient Feature Selective Validation (FSV) techniques to undertake this analysis with an emphasis on transient data processing. The nature of FSV makes it a natural technique to consider for this problem space. Open questions have existed as to how transients should be dealt with in FSV. This paper overcomes the limitations of previous approaches for step-function transient comparison and presents analytical methods to ensure the transient feature itself is considered, irrespective of how much pre- and post- transient data happens to be included.

1. Introduction

As large-scale wind farms move further offshore, cost effective Condition Monitoring (CM) plays a crucial role in minimizing Wind Turbine (WT) operations and maintenance costs for a competitive development of wind energy [1,2]. WTs experience a broader range of dynamic loads than most other large conventional rotating machines. Transient events, occurring during control actions or anomalous wind speed behaviour, cause high loads and can lead to significant torque reversals that are harmful to drive train components and reduce their expected life [3,4]. Premature gearbox bearing failures have been associated with overloading experienced by the drive train [5,6]. As the loading on the WT drive train components is highly variable, the study of transient conditions is fundamental to the development of reliable CM techniques. Mechanical torque measurements offer a holistic CM view by providing an insight into WT energy conversions and are excellent candidates for improving condition monitoring. The potential of monitoring different WT drive train components using direct measurements of the shaft mechanical torque signal is significant, as it contains information on the machine mechanical response to wind before any generator effects.

WT component faults have usually distinguishable mechanical torque signatures and therefore can be diagnosed by using torque signals [7]. Shaft torque directly reflects force exchanges in the drivetrain, as well as their effect on the main drivetrain components. This is a significant advantage when compared to indirect parameters related to the reaction of components to forces, such as vibration measurements on bearings or gears. The potential benefits of adopting CM techniques based on WT mechanical torque measurement have been shown for the detection of generator electrical faults [8,9], drive train mass imbalance [10], gearbox failures [11], blade mass imbalance and aerodynamic asymmetry [12,13]. Besides enhancing WT CM capabilities, direct high-frequency real-time reliable measurements of drive train loads can improve confidence in drive train design as well as allow the adoption of proactive solutions for extreme load mitigation. However, torque measurement on such large, inaccessible machines is impractical and economically infeasible, mainly due to limitations of the specialized equipment currently available. Methods for shaft torque measurements are complex and tend to lack robustness when used in a long term configuration. Direct methods use in-line torque transducers, already calibrated by the manufacturer, which are integrated into the drive shaft. These sensors have some susceptibility to noise and require bearings for support, which also implies maintenance. The major obstacle to the industrial application of direct measurement systems is the costly and intrusive nature of

the equipment, which is impractical on large systems. Measurements of shaft torque in industrial applications are today most often done by strain gauges directly bonded on the rotating shaft. The main limitations of this method are the complexity of installing sensors and electronics on the rotating shaft as well as the transfer of the measured signals through a wireless connection or slip rings. Moreover, unwanted forces can create unintended directional disturbance, such as crosstalk phenomena, that can increase the uncertainty in the measured loads and reduce accuracy [14]. A novel contactless measurement system for direct, low-cost real-time measurement of WT drive train loads and speed has been presented and experimentally validated in [15]. The proposed technique is based on the measurement of the shaft angle of twist between two points on the shaft, separated by a suitable distance, through optical angular position sensing. The principle of the proposed method is to quantify the shaft relative twist angle due to torsional effects by measuring the phase difference between two pulse signals recorded by the optical sensors and hence deriving the applied torque. The twist angle-torque characteristic can either be mechanically calibrated or calculated. Unlike conventional in-line torque transducers [16–18], the proposed contactless measurement system can be designed to be fitted or retrofitted on any shaft diameter and material without mechanical interference. Unlike conventional strain gauge techniques, the proposed torque meter does not require costly embedded sensors, electronics or wires on the rotating shaft. Its performance and accuracy have been experimentally demonstrated under dynamic, transient loads through conventional visual comparison and signal Root Mean Square Error (RMSE) calculations against measurements from an intrusive reference state-of-the art transducer [19]. The principal issue here is that a visual comparison is still a key part of the assessment process. This paper further validates the proposed contactless technique through an objective, quantified, comparison of the transient load and speed measurements based on an enhanced transient Feature Selective Validation (FSV) approach.

FSV was chosen for this work because it has been shown to provide a quantitative comparison of visually non-trivial, graphically presented, data that emulates the range of qualitative opinions of a group of experts. Thus reducing the reliance on visual assessment of an individual expert, with the inherent variation between individuals not being accounted for, by providing a proxy for a panel of experts and giving an indication of the range of opinions that such a panel might come to. As such, it has been demonstrated to provide support for quality-of-results decisions similar to having a team of experts look at the data. It does this through a heuristic approach rather than an artificial intelligence approach. The primary applications for FSV have been in Electromagnetic Compatibility (EMC) and signal / power integrity, but with a hitherto unsolved problem of how to adequately compare step transient data, such as that occurring for power or logic switching. This EMC related data is structurally very similar to that of the torque data of interest to the wind turbine design and maintenance community and, hence, a natural approach to use: if a method to compare step transient data can be introduced and verified. This paper presents this solution.

It is known that visual evaluation is the most subtle and widely used method of data comparison and validation [20,21]. However, visual assessment is prone to many types of physical and psychological influences. For these reasons, the FSV method was established to support the validation of electromagnetic models by quantifying the agreement between the reference and the numerical results. Where the aim was to mirror, as far as possible, the opinion of a large group of expert users as a whole. This method has been incorporated as the central technique of IEEE Standard (STD) 1597.1 and its associated Recommended Practice Guide,

1597.2 [22,23]. The details of the FSV method and its latest applications can be found in [24,25].

The FSV method was developed using a reliability function philosophy to overcome some of the key problems associated with validation of computational electromagnetic simulations for EMC problems. Key amongst those problems is that the complexity of the systems being analysed resulted in visually complex graphical data with a definable envelope and many fast-moving resonant like features. The challenge was increased by the need for simulations to be much simpler than the measurement environment. One of the most significant difficulties was that many of the experts would interpret the data differently based on their backgrounds and expectations (for example, someone from an EMC measurement background may have a different interpretation of what 'good agreement' might be compared to someone from a radiofrequency design background). As a result, the FSV method was developed to provide a 'probability' density function that closely resembles that derived from a group of experts. From this, a mean or mode can be obtained to summarize the view of experts [21]. The original formulation was based on the comparison of x-y data with no meaning derived from the units of either axis. A significant short-coming of the original FSV formulation was that, when applied to transient data, the length of time included in the pre- and post-transient phases could inadvertently (or purposely) dominate the transient itself. A further shortcoming was identifying the start and end of the transient (for the purposes of comparison). A transient FSV algorithm was developed which looked at impulsive-like transients but was insufficient to adequately capture the effects of switching or step-like transients. However, for the emulated torque data of wind turbines, the comparison between step-function transients is essential and a new challenge for the FSV method. This paper develops the generalized FSV method to include an approach that satisfies the step-function requirements to allow transient data to be compared.

The structure of this paper is as follows. In Section 2, the basic algorithms of FSV and the problems of transient FSV are reviewed. The generalized transient FSV approach is presented and validated in Section 3. The proposed method is applied to emulated wind turbine torque data in Section 4.

2. Overview of the FSV technique

2.1. Standard FSV method

The FSV method provides detailed, point-by-point comparisons of the 'envelope' of the two data sets being considered and the fine-grained detail as two separate comparisons. These are then combined into a 'global' comparison. This point-by-point data can then be used to generate a probability distribution, which is useful for statistical analysis of data comparisons, histogram charts related to expert opinion or single goodness-of-fit values for more deterministic quantitative use.

A graphical demonstration of the FSV 'data flow' is provided in Fig. 1. The original data for comparison (Fig. 1(a)) was obtained from coupling measurements in a mode-stirred reverberation chamber with slightly different positions of the mechanical stirrer. The axes are arbitrary units in that the x-axis is the frequency point number (not the actual frequency, as FSV works on points not frequencies) and the y-axis is the S_{21} parameter in linear units, effectively the proportion of signal that was transmitted that couples back into the measuring equipment (a vector network analyser). It should be noted that the method is domain-agnostic, so no information is derived from the axes units. Three figures of merit are obtained to demonstrate data agreement from different

(a) Original data for comparison (axes are arbitrary units)

(b) Amplitude Difference Measures

(c) Feature Difference Measure

(d) Global Difference Measures

(e) GDM histogram

(f) GDM histogram compared to (group) visual assessment

(g) GDM density function

(h) GDM cumulative density function, showing maximum 'D' parameter for Kolmogorov-Smirnov analysis
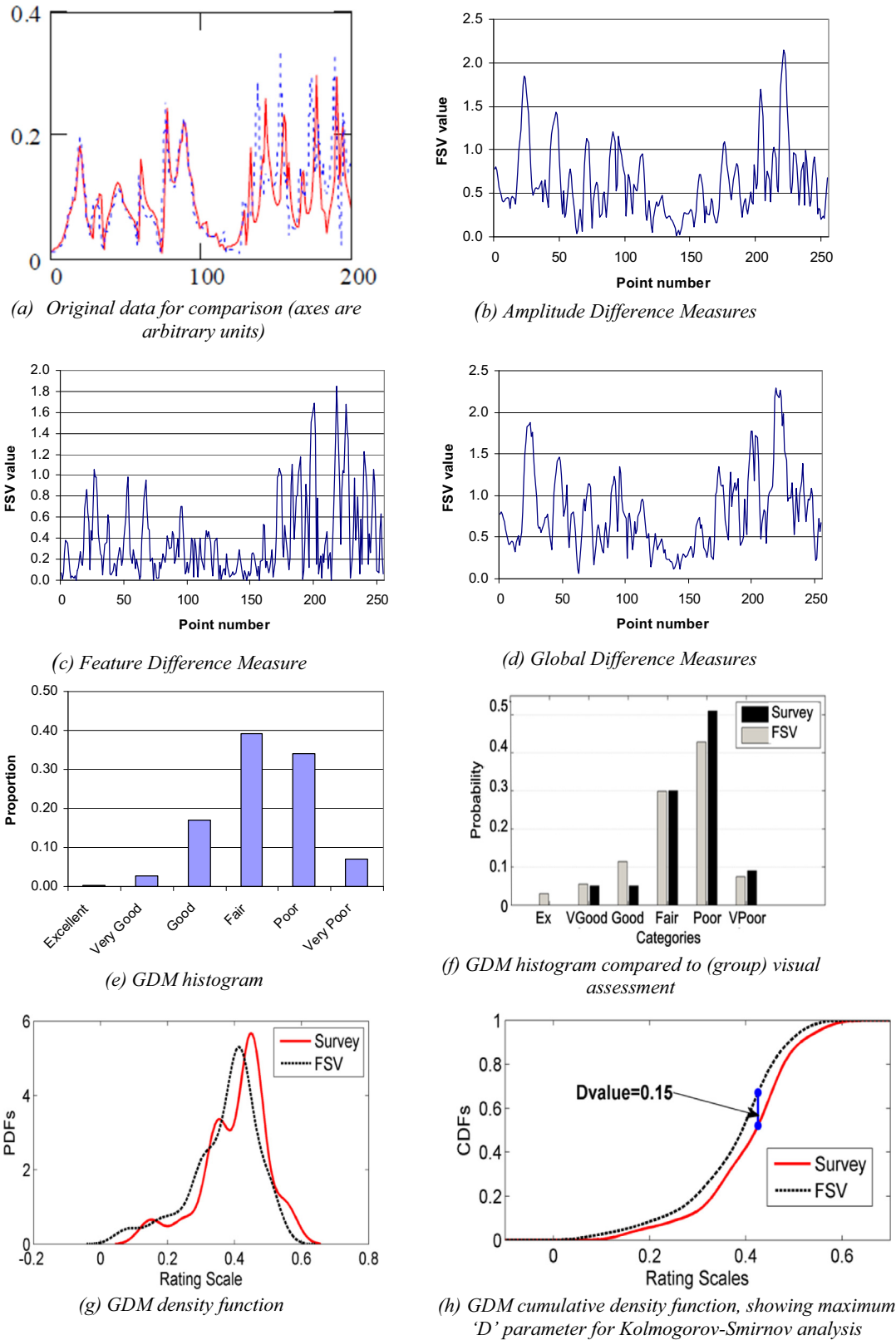
Fig. 1. Summary of FSV.

perspectives in the FSV method. The Amplitude Difference Measure (ADM) shows the 'trend' difference (Fig. 1(b)), while the Feature Difference Measure (FDM) denotes the differences of details (Fig. 1(c)). Then the ADM and FDM are combined to give the Global Difference Measure (GDM) (Fig. 1(d)). Further, in order to provide a direct link with visual assessment, the point-by-point FSV outputs are binned into a confidence histogram (usually labelled ADMc, FDMc and GDMc). The GDMc is shown in Fig. 1(e). This data can

be used as a proxy for the qualitative assessment of a group of experts relating the quantitative FSV output to qualitative natural language descriptors (excellent, very good, good, fair, poor, very poor). The FSV output is compared with the opinions of a group of 50 engineers in Fig. 1(f). The FSV data can also be represented as a density function (Fig. 1(g)) which enables a statistical analysis of the comparison data [26] or can be useful for further meta-comparisons, such as in Fig. 1(d), where the cumulative density function is being used to verify with a Kolmogorov-Smirnov test the hypothesis that the visual and FSV data are from the same distribution. For this data D_{crit}, the value at which the difference in amplitude is such as to reject the null hypothesis, for 90% confidence is 0.17, so the null hypothesis can be accepted – a common trend when comparing FSV data and visual assessment, and hence one reason for considering FSV for the analysis of WT transient data.

The formulation of FSV was heavily influenced by the approaches used by Zanazzi and Jona, van Hove, and Pendy [27]. The standard FSV procedures are as follows.

1) Data segmentation

The purpose of this action is to filter the data from each data set to be compared into low pass, band bass and high pass components. Other approaches may be used but the method here, and commonly used in the community, is to Fourier Transform the data, mask it into the three regions and then Inverse Fourier Transform into the original working domain. This can be applied to any working domain (time, frequency, distance, angle, etc.) To achieve this, the working datasets under comparison are first Fourier transformed. Then, the filter shown in Fig. 2 is applied to the transformed working datasets to obtain the DC, Low-, and High-frequency components. The 'break-point' location, N_{bp}, is decided by

$$\sum_{i=N_{DC}+1}^{N_{40\%}} TDWS(i) \leq 0.4S \tag{1}$$

$$N_{bp} = N_{40\%} + 5 \tag{2}$$

where $TDWS(i)$ is the value of the ith independent variable within the Fourier transformed data set; S is the sum of the values of the independent variable; N is the sum of the values of the independent variable; $N_{40\%}$ is the element containing the '40% location'. The 'break-point' location N_{bp} is five data points higher than the '40% location'. N_{DC} is set to 4. A "breakpoint" at five data points above $N_{40\%}$ allows a comfortable transition window between the low and the high results. The windowed frequency components are then inverse transformed to obtain DC, Low and High components, labeled as DC, Lo and Hi, respectively.
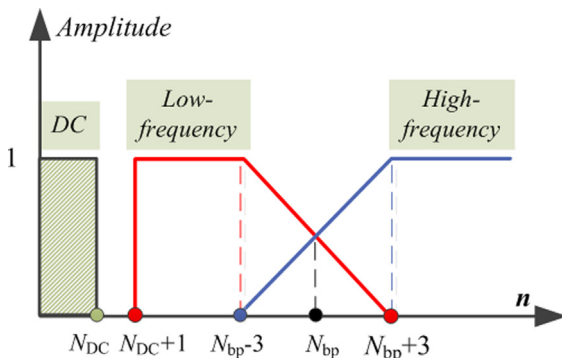
Fig. 2. Filter used in the original FSV method [28].

2) The calculation of ADM

The ADM is calculated to show the difference between DC and low-frequency information in both of the datasets under comparison.

$$ADM(n) = \frac{||Lo_1(n)| - |Lo_2(n)||}{\sum_{i=1}^{N}(|Lo_1(i)| + |Lo_2(i)|)} + ODM \tag{3a}$$

where

$$ODM(n) = \left|\frac{\chi}{\delta}\right| exp\left\{\left|\frac{\chi}{\delta}\right|\right\} \tag{3b}$$

$$\chi = (|DC_1(n)| - |DC_2(n)|) \tag{3c}$$

$$\delta = \frac{1}{N}\sum_{i=1}^{N}(|DC_1(i)| + |DC_2(i)|) \tag{3d}$$

where N is the sum of the values of the independent variable; n is the nth data point. The FSV measures are generally based on a 'difference over sum' approach, except the ODM: the use of the exponential reflects the non-linear interpretation of offsets in data, where a small offset is frequently ignored but a large offset is regarded as significant, even if the original data is highly similar in shape.

3) The calculation of FDM

The scaling factors 2, 6, and 7.2 in Eqs. (4), (5) and (6) are used to balance the internal sub-measures of the FDM, emphasizing either low level trends (broad peaks/troughs) or higher level features (narrow peaks/troughs).

$$FDM_1(n) = \frac{\left|Lo_1'(n)\right| - \left|Lo_2'(n)\right|}{\frac{2}{N}\sum_{i=1}^{N}\left(\left|Lo_1'(i)\right| + \left|Lo_2'(i)\right|\right)} \tag{4}$$

$$FDM_2(n) = \frac{\left|Hi_1'(n)\right| - \left|Hi_2'(n)\right|}{\frac{6}{N}\sum_{i=1}^{N}\left(\left|Hi_1'(i)\right| + \left|Hi_2'(i)\right|\right)} \tag{5}$$

$$FDM_3(n) = \frac{\left|Hi_1''(n)\right| - \left|Hi_2''(n)\right|}{\frac{7.2}{N}\sum_{i=1}^{N}\left(\left|Hi_1''(i)\right| + \left|Hi_2''(i)\right|\right)} \tag{6}$$

$$FDM(n) = 2(|FDM_1(n) + FDM_2(n) + FDM_3(n)|) \tag{7}$$

where $Lo_{\{1,2\}}'$ and $Hi_{\{1,2\}}'$ are the first derivatives of the $Lo_{\{1,2\}}$ and $Hi_{\{1,2\}}$ components, respectively; $Hi_{\{1,2\}}''$ is the second derivative of the $Hi_{\{1,2\}}$ component. The sub-level difference measures in Eqs. (4), (5), and (6) emphasize independent areas of the compared signals.

4) The Global Difference Measure (GDM) is obtained through combination of the ADM and FDM. The GDM gives an indication of the overall goodness-of-fit of both amplitude and feature differences between compared signals, quantifying the overall assessment of a comparison.

$$GDM(n) = \sqrt{ADM(n)^2 + FDM(n)^2} \tag{8}$$

5) The original development of FSV looked to bridge the gap between a quantitative assessment and the subjective, qualitative, assessment common in papers, presentations and

reports thought the use of a natural language interpretations scale. The FSV interpretation scale is shown in Table 1. In this way, the form of qualitative result, xDMc (where x is A, F or G), becomes a six-category confidence histogram.

To some extent, this approach is being superseded by the use of density functions and distributions, which provide more options for analysis, particularly meta-comparison. However, the interpretation scale is still widely used and it is common to see such interpretations in papers where FSV is used. The qualitative interpretations are not intended to be absolute definitions of quality, they are merely a means to aid human communication.

2.2. Transient FSV method

The comparison of transient data is made more difficult by the indeterminate nature of the 'pre' and 'post' transient regions, as shown in Fig. 3(a). In essence, a comparison could be dominated by the selection of the length of the tails either side of the transient event. This has recently received some attention [29–31] with the identification of weighting regimes to ensure that the transient event itself dominates any comparison and such a comparison is not skewed by arbitrary choice of duration. Reference [29] also provided some indication of where experienced users of transient data would place those boundaries.

A segment approach was proposed in [29], algorithms were designed to divide the transient into three regions: pre-transient event, transient event and post-transient event. FSV is applied in each region separately. Then, the values of the three regions are combined and each region is weighted according to its importance in the analysis. The transient region was originally considered as ranging from the end of the pre-transient up to a point that contains 65% of the signal's energy. The energy is calculated by

$$Energy_{\{1,2\}}(n) = \sum_{i=1}^{n} \left(Data_{\{1,2\}}(i)\right)^2, n = 1, 2, 3, \cdots..N \tag{9}$$

where $Data_{\{1,2\}}$ is the set of the data to be compared ("1" is the first dataset and "2" the second dataset) and N is the length of $Data_{\{1,2\}}$.

It is clear that this approach is valid for the transient in Fig. 3(a), but is invalid for the step transient in Fig. 3(b) since the energy will be concentrated in the pre-transient region rather than the transient region (or vice versa). The approach to transients used in Fig. 3(a) is based on the energy being concentrated in the transient region, something that does not happen with a step-function type transient.

3. Generalized transient data method

To overcome the problems of transient FSV in applications, such as torque data comparison, a generalized transient FSV approach is required. Such an approach is proposed and tested here. This generalized approach aims to compare the transient data using the standard FSV method after pre-processing. Meanwhile, the proposed approach is expected to be applicable to a wide variety of transient types, including those in Fig. 3. The key is to develop a

Table 1
FSV interpretation scale in [23].

FSV value y (quantitative)	FSV interpretation (qualitative)
y ≤ 0.1	Excellent
0.1 < y ≤ 0.2	Very Good
0.2 < y ≤ 0.4	Good
0.4 < y ≤ 0.8	Fair
0.8 < y ≤ 1.6	Poor
y > 1.6	Very Poor
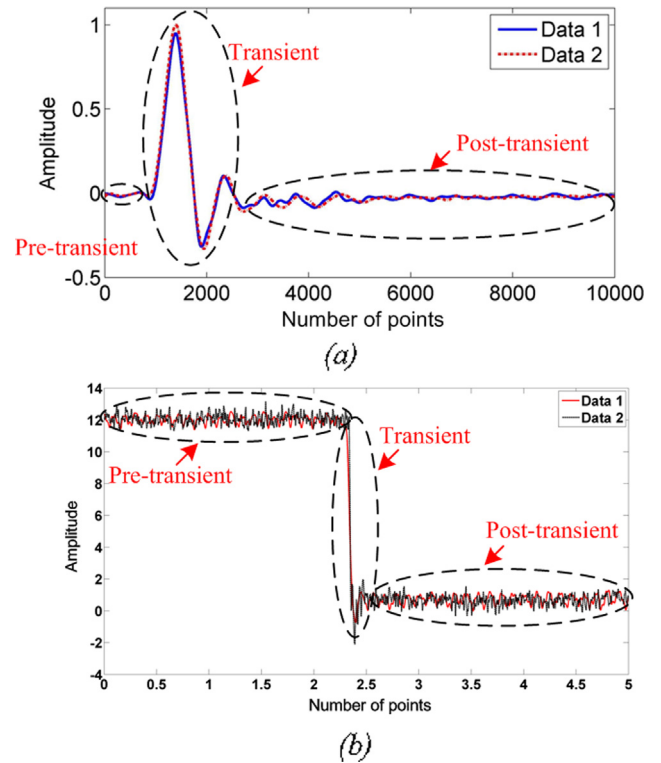
Fig. 3. Illustration of the regions of transient event.

pre-processing method that allows a clear identification of the boundaries between the pre-transient/transient and the transient/post-transient regions.

3.1. Generalized transient FSV method

Step 1: The boundaries of pre-transient, transient and post-transient regions are identified. To find the boundaries of "step transient signals", such as that shown in Fig. 3(b), the derivative of datasets under comparison are calculated and the boundaries are determined according to the Cumulative Distribution Function (CDF) of data 1 and data 2.

1. The cumulative distribution is calculated by

$$E(n) = \sum_{i=1}^{n} \left(Data_1'(i)^2 + Data_2'(i)^2\right), n = 1, 2, 3, \cdots..N \tag{10}$$

where $Data_{\{1,2\}}'$ is the derivative of the data to be compared ("1" is the first dataset and "2" the second dataset). N is the length of $Data_{\{1,2\}}'$.

2. Then the least-squares fit of a straight line to the cumulative distribution, $E(n)$, is calculated. $E(n)$ is then de-trended by subtracting the resulting least-squares function from the original data. $E(n)$ is de-trended by

$$E_{detrend}(n) = E(n) - (an + b), n = 1, 2, 3, \cdots..N \tag{11}$$

where a and b are the coefficients of a straight-line function $(an + b)$ that fits $E(n)$.

3. Subsequently, the positions of the turning point (crest and trough of the de-trended data $E_{detrend}(n)$), N_{bp1} and N_{bp2}, are found and they are chosen as the pre- and post-transient boundaries.

The process to identify the breakpoints of a pair of step transient data and a pair of normal transient data is shown in Fig. 4 and Fig. 5, respectively.
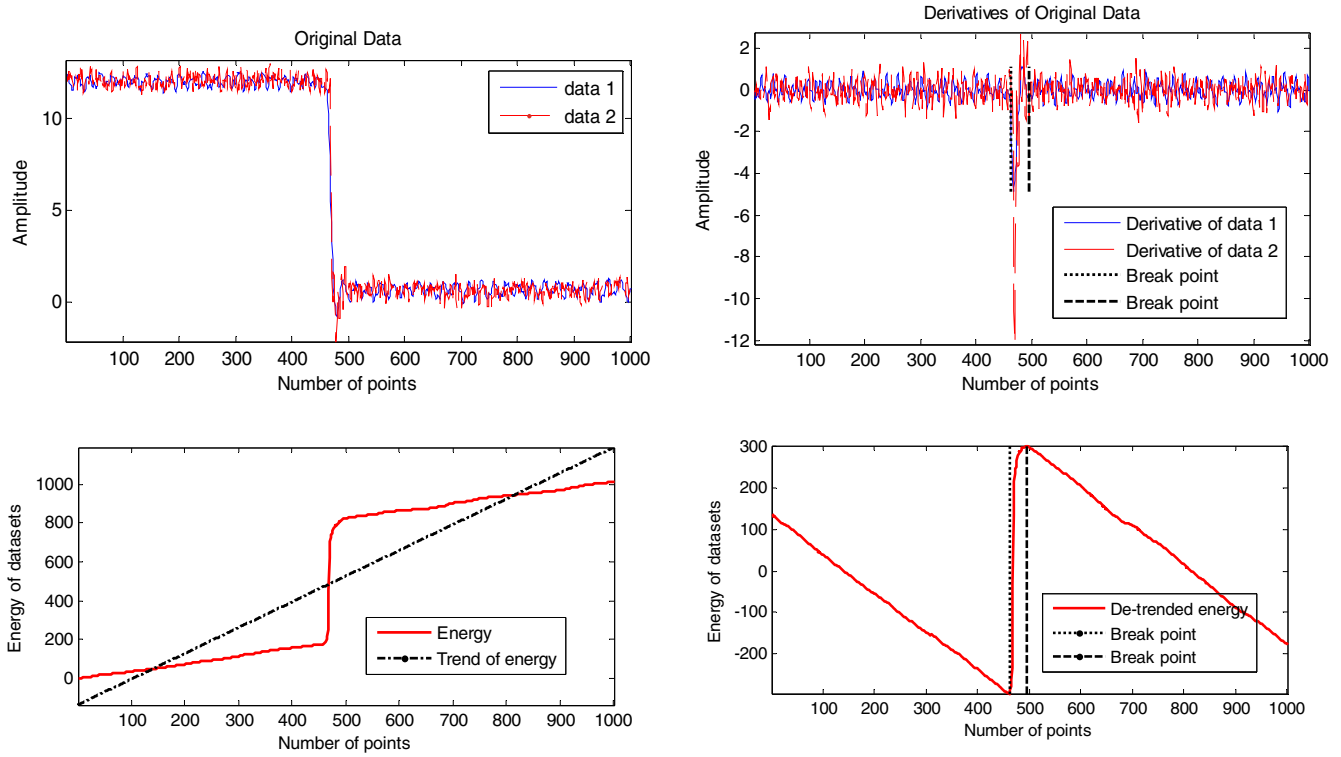
Fig. 4. Break-point selection of the step transient data. Note the indication of the trends and break points.
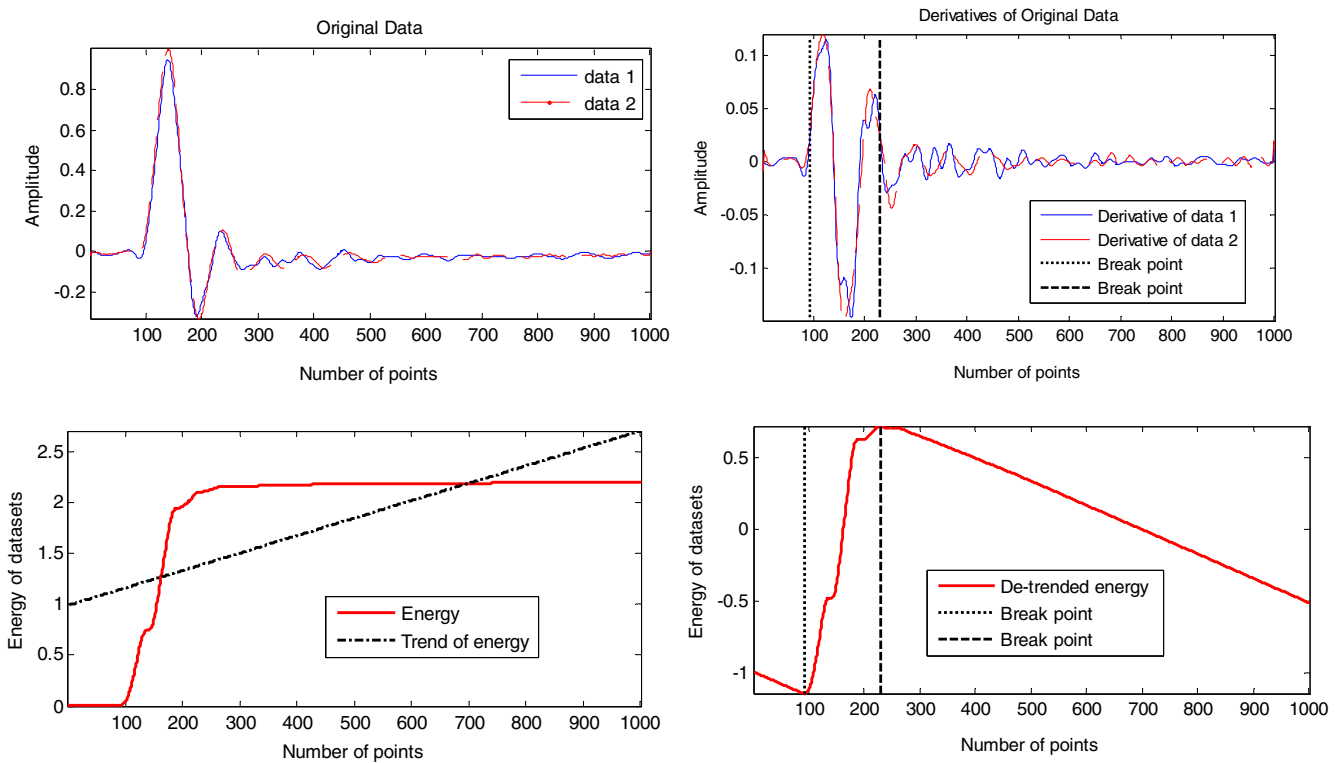
Fig. 5. Break-point selection of the normal transient data. Note the indication of the trends and break points.

Step 2: Instead of the weighting approach proposed in [29], a pre-emphasis approach that is based on interpolation of points in the three regions to match the weighting functions is proposed. Effectively the pre-transient, transient and post-transient regions are expanded or contracted to match the influence the regions have on the overall results. The lengths of pre-transient and post-transient regions are proposed to contributing 5% and 20% percent of the overall weighting of the comparison whole length, respectively, as shown in Fig. 6.

The values of 5% and 20% are based on the experience of the authors and are values that can be subject to further investigation:
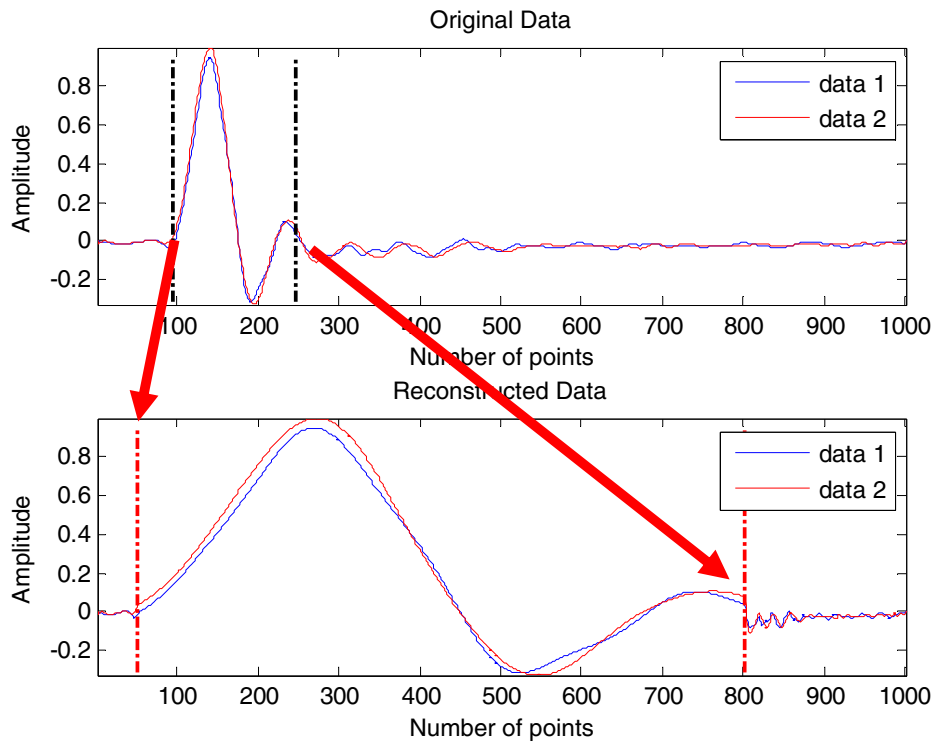
Fig. 6. Illustration of the pre-emphasis approach to data based on interpolation of points in the three regions.
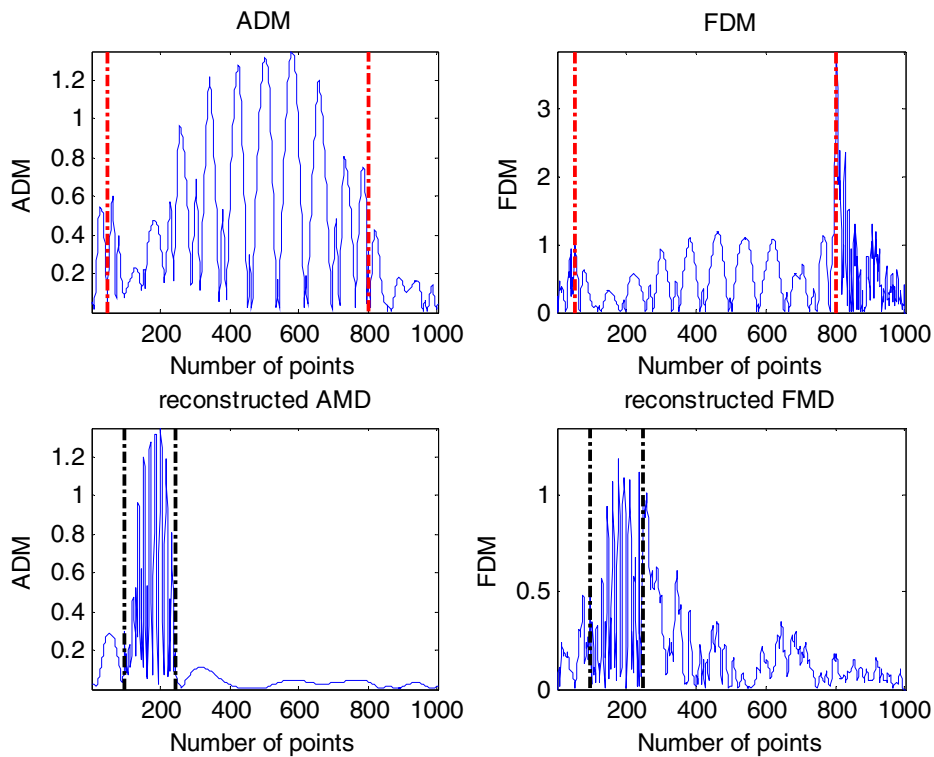
Fig. 7. Re-mapping point by point FSV result back to the original data point.

the authors would welcome further research and contribution to this from the wider community. The "companded" data sets are then compared using the standard FSV method. The ADM and FDM results are shown in Fig. 7, which also shows the re-mapping used to provide the emphasis of the regions just described. Hence, the pre-transient region is compressed (or expanded) to occupy 5% of the data points. In the example of Fig. 7, this will be 50 points. The transient region is expanded (or compressed) to occupy 75% of the data points (750 points in this case) and the post-transient region will occupy the remaining 20% of the points. This approach has the benefit of not requiring separate comparisons that are then 'stitched' back together but treats the overall comparison as a single uniform whole which can then be interpolated back to the original point distribution.

Step 3: Re-mapping point by point data back to the original data point distribution using the interpolation in reverse. The reconstructed ADM and FDM are obtained by expanding (or compressing) the FSV results in pre-transient and post-transient regions to return to the original point density. The amplitude of the ADM

and FDM in pre-transient and post-transient regions are proportionally varied. The proportionality factor is obtained by

$$P = \frac{Nc}{No} \tag{12}$$

where Nc is the length of the compressed (expanded) region and No is the length of the original region. Then the GDM is calculated by (8).

3.2. Performance test

The standard and transient FSV has used visual assessment surveys to verify its performance [29,31]. Since the survey results are qualitatively presented by natural language descriptors, the survey results are first transformed into quantitative results according to Table 1. After that, the statistics, mean and standard deviation, of GDM and survey results are calculated. The comparison between standard deviations indicates whether FSV and the visual assessments are within each other's range of expectation.
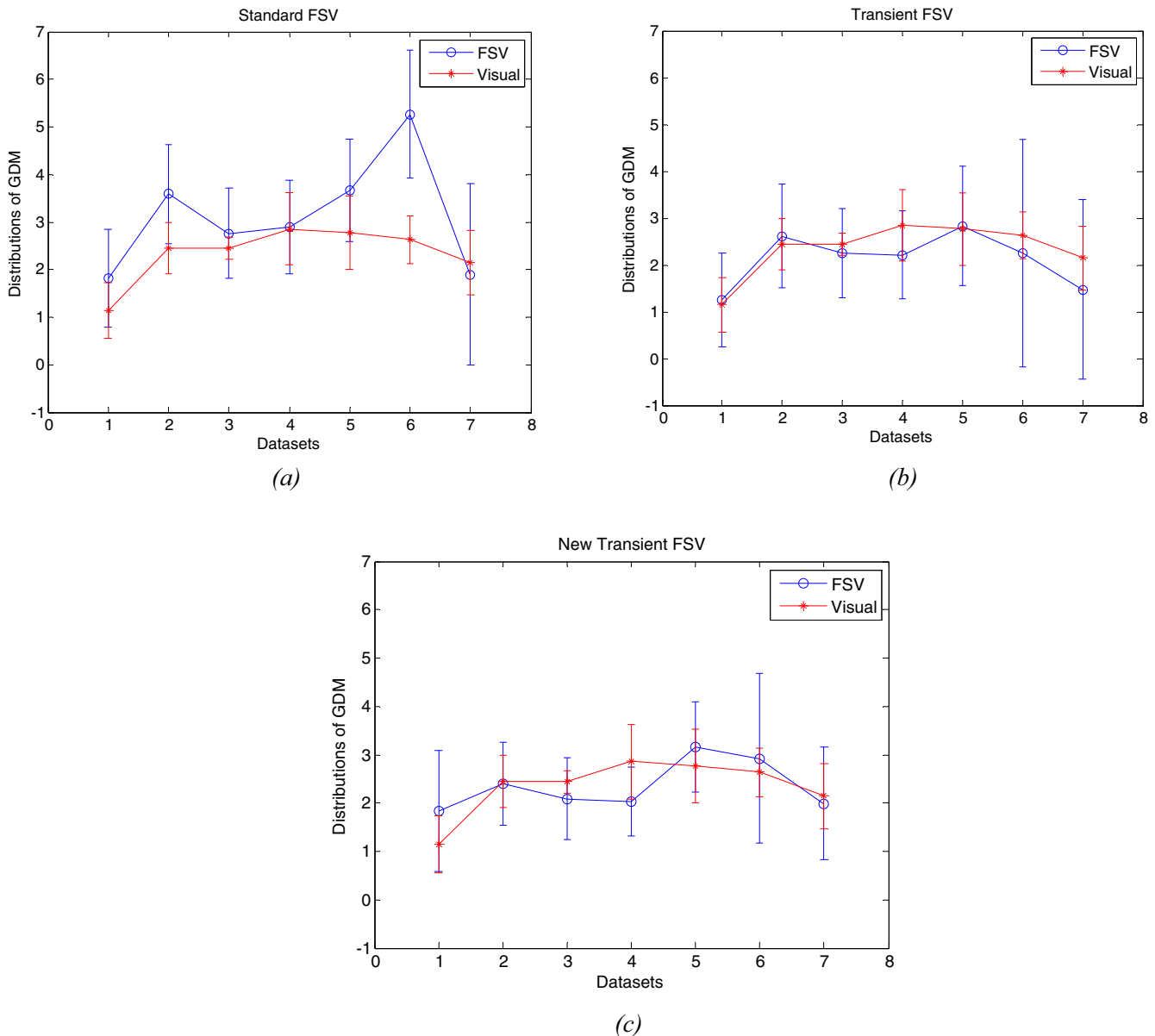
Fig. 8. Comparison between 2011 survey and FSV results, (a) standard FSV, (b) transient FSV, (c) generalized FSV.

Table 2
Comparison of mean and standard deviation values of GDM for 2011 survey data.

Statistics of GDM	Methods	Transient data sets						
		1	2	3	4	5	6	7
Mean value	Visual assessment	1.15	2.44	2.44	2.85	2.77	2.63	2.15
	Standard FSV	1.83	3.59	2.76	2.90	3.68	5.27	1.90
	Transient FSV	1.24	2.62	2.25	2.21	2.83	2.24	1.47
	Generalized FSV	1.84	2.39	2.09	2.04	3.15	2.92	1.99
Standard deviation	Visual assessment	0.59	0.54	0.24	0.76	0.77	0.50	0.68
	Standard FSV	1.03	1.04	0.95	0.98	1.08	1.34	1.91
	Transient FSV	1.00	1.11	0.96	0.95	1.28	2.43	1.92
	Generalized FSV	1.25	0.86	0.85	0.71	0.94	1.76	1.17

The generalized transient FSV method is tested using the transient data in [29] that comprises 7 typical (non-step) transient structures. The results of standard FSV, transient FSV and the generalized transient FSV method proposed in this paper are compared in Fig. 8 (in the same y-axis range). The mean and standard deviation values are presented by error bars.

It is demonstrated in Fig. 8 that both the transient FSV and generalized FSV method could reduce the disagreement between FSV and visual assessment. Overall, there is little difference in the means of the comparisons between the original transient and the generalized transient approaches, which supports the generality of use proposition. Both are significantly better than the standard

FSV approach itself. Relevant data including average value and standard deviation are given in Table 2 to show the experimental results more specifically.

Also, the performance of the new transient FSV method for the ordinary datasets in [32] were also tested, as shown in Fig. 9. Specifically, the average and standard deviation values are outlined in Table 3. It is noted that the generalized FSV method has little influence on the assessment of the ordinary datasets, further supporting the thesis that the method proposed in this paper can be more widely applied irrespective of the nature of the original data. This is attributed to the fact that the pre-processing of the generalized FSV has little influence on the ordinary datasets.

(a)

(b)
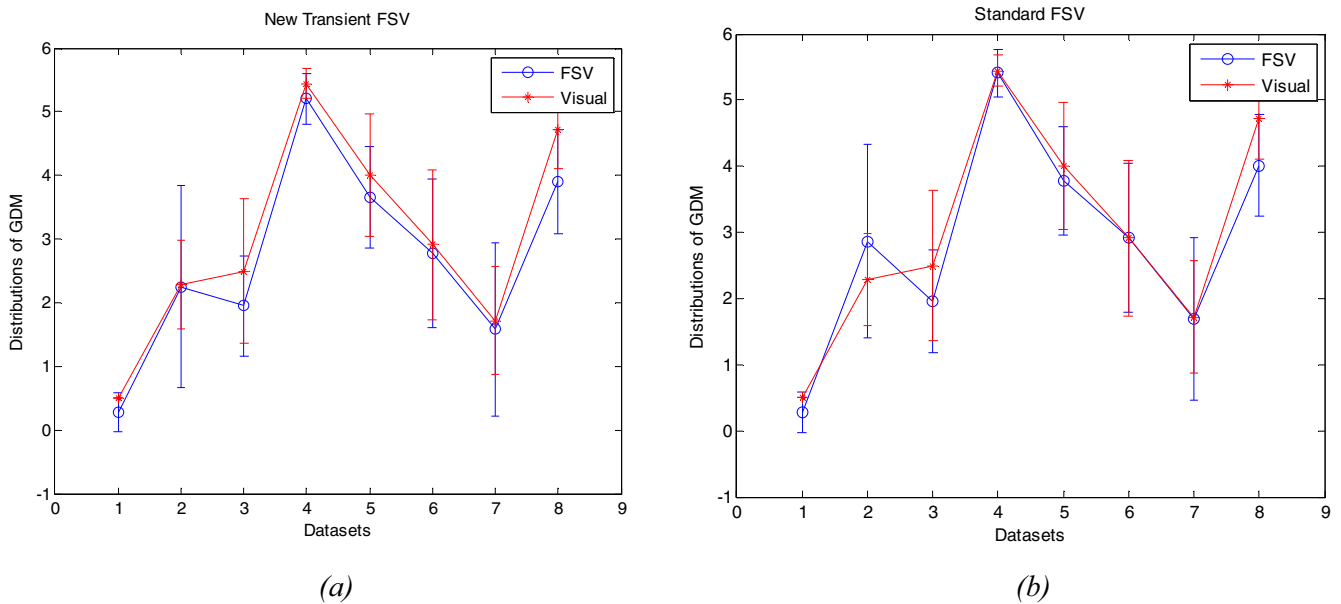
Fig. 9. Comparison between 2014 survey and FSV results, (a) generalized FSV, (b) standard FSV.

Table 3
Comparison of mean and standard deviation values of GDM for 2014 survey data.

Statistics of GDM	Methods	Data sets							
		1	2	3	4	5	6	7	8
Mean value	Visual assessment	0.50	2.28	2.50	5.44	4.01	2.91	1.72	4.72
	Standard FSV	0.28	2.87	1.96	5.41	3.78	2.92	1.68	4.01
	Generalized FSV	0.28	2.25	1.95	5.20	3.65	2.78	1.58	3.90
Standard deviation	Visual assessment	0.00	0.69	1.14	0.24	0.96	1.17	0.85	0.61
	Standard FSV	0.30	1.46	0.79	0.36	0.83	1.13	1.23	0.77
	Generalized FSV	0.30	1.59	0.79	0.41	0.81	1.16	1.36	0.81

4. Results

Step transient speed and torque data was experimentally obtained by emulating shaft dynamic transient loads experienced by a WT drive train on a small-scale test bench equipped with the contactless torque meter shown in Fig. 10 and described in detail in [19]. The rig features a 4-pole 5 kW Induction Motor (IM) driving a 4-pole 5 kW grid-connected Induction Generator (IG). The shaft speed profile is controlled by an ABB drive. The IG stator voltage, and hence the torque acting along the shaft, are varied using a variable transformer connected to the IG. The main shaft is instrumented at each end with a barcode with eight equal black–white segments. The barcode stripe pair number was selected as a trade-off between measurement uncertainty and computational cost. In correspondence to each bar code, an Optek reflective line reader sensor is mounted on a stationary rigid support, placed at the optimum distance of 0.76 mm from the target. The distance between the two optical sensors is 45.8 cm. shaft. As the shaft rotates, each optical sensor generates a pulse train signal proportional to the light intensity reflected by the barcode stripes. When a torque acts on the shaft, the relative rotation of the ends of the shaft section results in a time shift between the
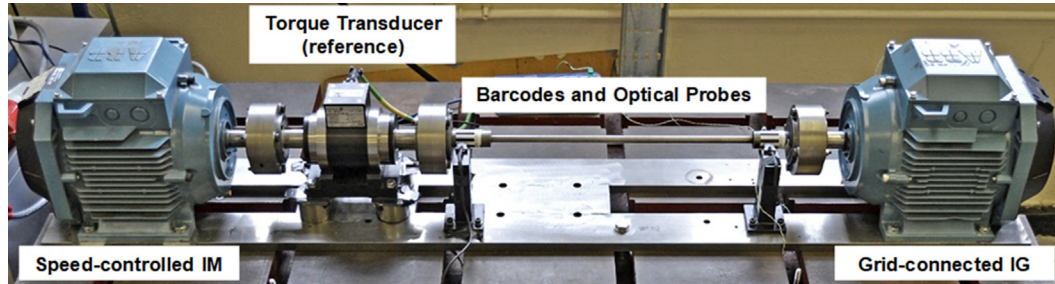
Fig. 10. Experimental test rig [19].
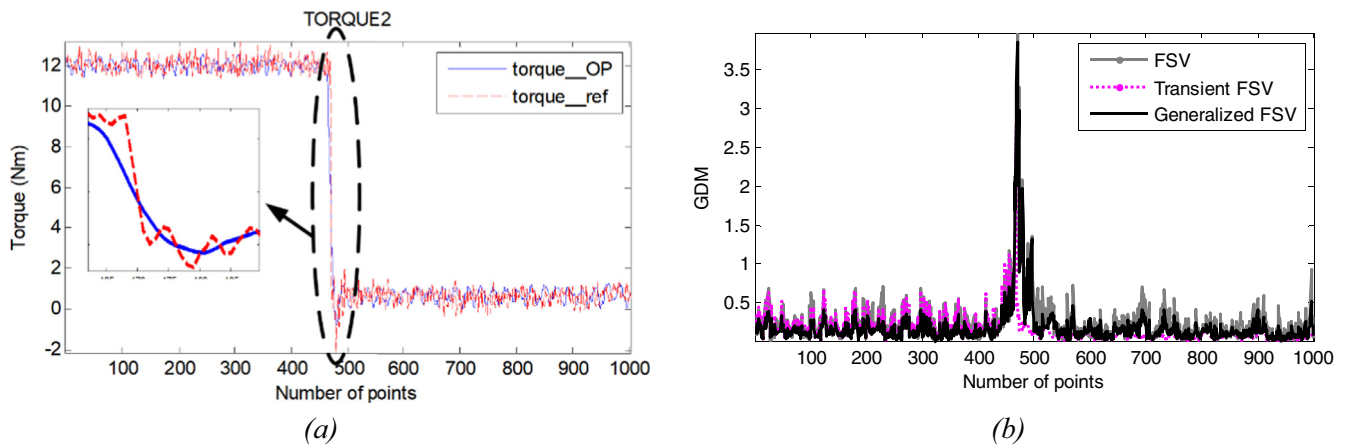
Fig. 11. (a) Experimental torque measurements; (b) Comparison of FSV results.
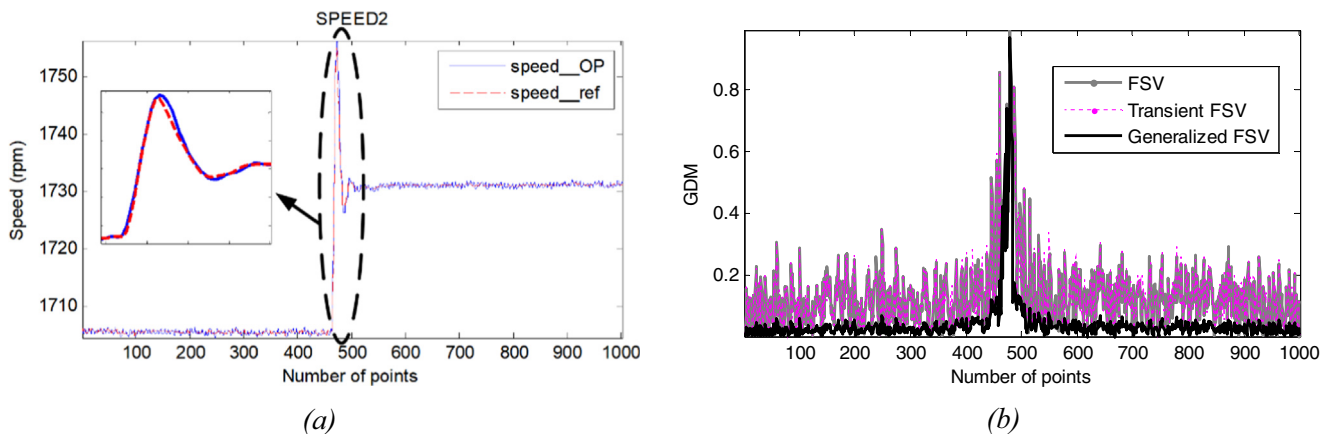
Fig. 12. (a) Experimental speed measurements; (b) Comparison of FSV results.

Table 4
Comparison of GDMtot and KS-test results given by different FSV algorithms.

| Methods | GDMtot | | KS-test results (statistic D) | | | | | |
| | Torque | Speed | Torque | | | Speed | | |
			Standard FSV	Transient FSV	Generalized FSV	Standard FSV	Transient FSV	Generalized FSV
Standard FSV	0.26	0.13	–	0.31	0.13	–	0.01	0.67
Transient FSV	0.14	0.13	0.31	–	0.24	0.01	–	0.67
Generalized FSV	0.18	0.04	0.13	0.24	–	0.67	0.67	–
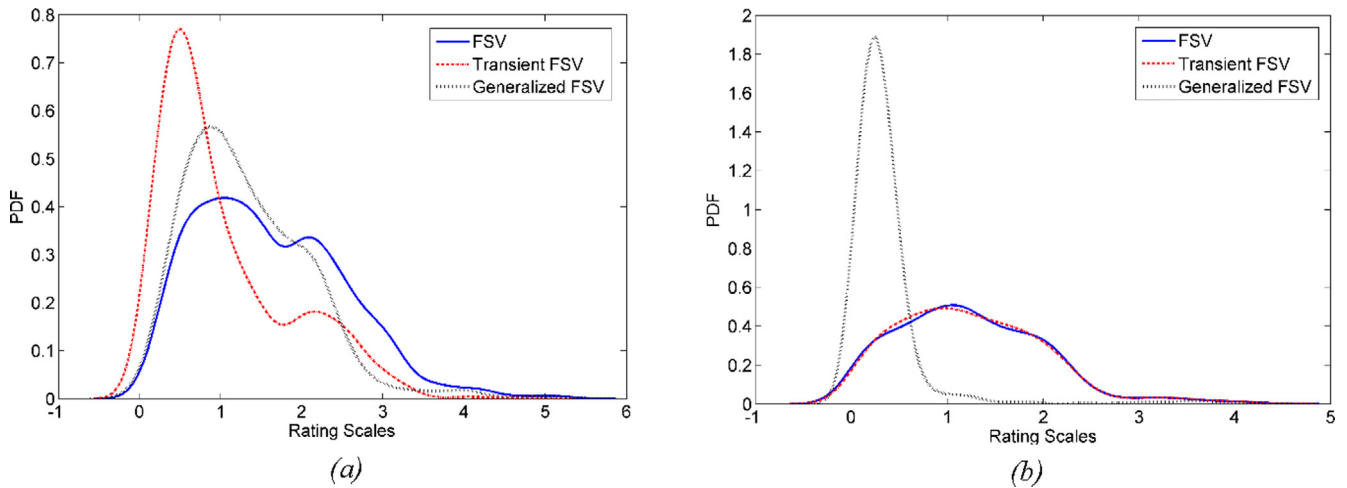
Fig. 13. Comparison of PDFs of GDM for (a) torque measurements; (b) speed measurements.

two pulse train signals. Torque and speed measurement is achieved by estimating the shaft twist angle through analysis of the barcode pulse train time shifts [15]. An in-line Magtrol TMB 313/431 torque transducer is mounted on the test bench and, being a well-established state-of-the-art technique, it has been assumed as the reference measurement system during the experimental campaign. Signals from the optical probes and the reference torque transducer are acquired by a PicoScope 4824 oscilloscope, with 100 kHz sampling frequency.

Experiments have been performed to emulate shaft dynamic transient loads experienced by a WT drive train, during anomalous wind speed fluctuations and control actions. The effects of torque reversal due to a drastic reduction of the shaft load, as typically occurring in WT stopping events, are shown in Fig. 11(a). The corresponding changes in speed, shown in Fig. 12(a), are the result of the applied torque that was not countered by the variable speed drive connected to the rig induction motor. Both figures show the contactless torque meter measurements (in blue) compared with those of a reference in-line torque transducer (in red). In both cases, the data comparison visual evaluation shows good agreement between measurements with signal RMSE values of 0.53 Nm and 0.45 rpm, respectively.

The torque and speed data comparison when applying the standard FSV, transient FSV and generalized FSV method, are shown in Fig. 11(b) and 12(b), respectively. The lower values of the generalized FSV, compared with the standard and transient FSV approach in the pre- and post-transient regions, show that the influence of noise is minimized in the comparison (as it is clearly the case for the speed FSV and (original) Transient FSV results in Fig. 12(b)). The GDMtot (the mean value of the GDM representing a single value goodness-of-fit measurement) of these methods is compared in Table 4. It is noted that the standard and generalized FSV

method could identify that the agreement between speed data is better than that of torque data, which could be verified by visual comparison of Fig. 11(a) and 12(a) as well as by the RMSE signal analysis results. However, the generalized FSV method results in FSV values that recognize the difference between the comparison between the speed and torque data. In contrast, the original transient FSV method is not as clear.

Also, the Probability Density Functions (PDFs) of GDM values given by different FSV algorithms are given in Fig. 13. The Kolmogorov-Smirnov test (KS-test) is applied to check if the distributions of two datasets are from the same distribution. The null hypothesis is that they are from the same distributions. The null hypothesis would be rejected if the test statistic, D, is greater than the critical value decided by significance level. The statistic D is determined by the maximum vertical deviation between the two curves of the Cumulative Distribution Functions (CDFs) of the datasets. In our case, the critical D value is 0.19 when significance level is set to 5%. The D values are outlined in Table 4. It is shown that the generalized FSV method outputs similar result with traditional FSV method for torque data. In contrast, the result of transient FSV method follows the same distribution with that of traditional FSV for speed data.

5. Conclusions

A generalized FSV approach is proposed to validate step-function transient data in WT measurement along with other data families. The approach is developed to overcome the limitations of previous standard and transient FSV methods. It is demonstrated that the proposed approach improves the performance of standard FSV method in the comparison of transient datasets and can be directly used in the comparison of ordinary (non-transient) data-

sets. Compared with to the transient FSV method, the generalized FSV method has been shown to adequately compare step-function transients. Further, the proposed approach ensures that the comparison is dominated by the transient function itself and not the length of the pre- and post-transient periods.

The proposed generalized FSV approach proves successful for an objective, quantified comparison of the speed and torque measurements from the innovative contactless torquemeter presented in this paper against measurements from a state-of-the art commercial intrusive sensor. This further validates and strengthen the outcomes from previously performed conventional visual and RMSE signal analysis. From the perspective of wind turbine data the use of FSV in the way suggested in this paper could improve condition monitoring via speed and torque data. The implementation of the contactless torquemeter in the field would allow to overcome the majority of problems currently limiting the industrial direct real-time measurements of WT drive train loads for CM purposes. Measurements at any point in time can be compared with a reference baseline measurement (perhaps installation conditions). This can be used to show if there is a drift by looking at the GDM and the size of the 1 standard deviation error bars over time. That possible variation over time can also be tested by undertaking a meta-comparison and applying something like the KS-test to provide a view on the level of significance to the differences in speed and torque measurements.

Acknowledgments

Declarations of interest

None.

References

[1] C.J. Crabtree, D. Zappalá, S.I. Hogg, Wind energy: UK experiences and offshore operational challenges, Proc. Inst. Mech. Eng., Part A: J. Power Energy 229 (7) (2015) 727–746.

[2] W. Qiao, D. Lu, A survey on wind turbine condition monitoring and fault diagnosis – Part I: components and subsystems, IEEE Trans. Ind. Electron. 62 (10) (2015) 6536–6545.

[3] D. Herr, Transient wind events and their effect on drivetrain loads Available at Windtech Int. 11 (3) (2015).

[4] J. Helsen, G. Van de Vyvere, K. De Bauw, P. Guillaume, Comparison of behaviour during torque reversal driven event on nacelle dynamometer and field turbine, in: Proceedings of the Conference on Wind Power Drives, Aachen (Germany), 2017, pp. 500–504.

[5] Y. Guo, J. Keller, T. Moan, H. Long, Model fidelity study of dynamic transient loads in a wind turbine gearbox, Proc. 2103 WINDPOWER Conference, Chicago, IL, 2013.

[6] E. Hart, A. Turnbull, J. Feuchtwang, D. McMillan, E. Golysheva, R. Elliott, Wind turbine main-bearing loading and wind field characteristics, Wind Energy 1–14 (2019), https://doi.org/10.1002/we.2386.

[7] W. Qiao, D. Lu, A survey on wind turbine condition monitoring and fault diagnosis – Part II: signals and signal processing methods, IEEE Trans. Ind. Electron. 62 (10) (2015) 6546–6557.

[8] S. Djurović, D. Vilchis-Rodriguez, A.C. Smith, Vibration monitoring for wound rotor induction machine winding fault detection, in: 2012 XXth International Conference on Electrical Machines, Marseille, 2012, pp. 1906–1912.

[9] D. Zappalá, N. Sarma, S. Djurović, C.J. Crabtree, A. Mohammad, P.J. Tavner, Electrical & mechanical diagnostic indicators of wind turbine induction generator rotor faults, Renewable Energy 131 (2019) 14–24.

[10] M.R. Wilkinson, F. Spinato, P.J. Tavner, Condition monitoring of generators & other subassemblies in wind turbine drive trains, in: 2007 IEEE International Symposium on Diagnostics for Electric Machines Power Electronics and Drives, 2007, pp. 388–392.

[11] H. Soker, S. Kieselhorst, R. Royo, Load monitoring on a main shaft. A case study, German Wind Energy Conference DEWEK, Wilhelmshaven, 2004.

[12] N. Perišić, P.H. Kirkegaard, B.J. Pedersen, Cost-effective shaft torque observer for condition monitoring of wind turbines, Wind Energy 18 (1) (2015) 1–19.

[13] D.J. Gardels, W. Qiao, X. Gong, "Simulation studies on imbalance faults of wind turbines, in: 2010 IEEE Power & Energy Society General Meeting, 2010, pp. 1–5.

[14] C.W. de Silva, Sensors and Actuators: Engineering System Instrumentation, second ed., CRC Press, Boca Raton, FL, 2015.

[15] D. Zappalá, M. Bezziccheri, C.J. Crabtree, N. Paone, Non-intrusive torque measurement for rotating shafts using optical sensing of zebra-tapes, Meas. Sci. Technol. 29 (6) (2018) 065207.

[16] G. Wegener, T. Bruns, Traceability of torque transducers under rotating and dynamic operating conditions, Measurement 42 (10) (2009) 1448–1453.

[17] R.S. Oliveira, S. Winter, H.A. Lepikson, T. Fröhlich, R. Theska, A new approach to test torque transducers under dynamic reference regimes, Measurement 58 (2014) 354–362.

[18] M. Chandra Sekhar Reddy, A.S. Sekhar, Detection and monitoring of coupling misalignment in rotors using torque measurements, Measurement 61 (2015) 111–122.

[19] D. Zappalá, C.J. Crabtree, S. Hogg, Investigating wind turbine dynamic transient loads using contactless shaft torque measurements, J. Eng. 18 (2019) 4975–4979.

[20] G. Zhang, L. Wang, X. Peng, A. Duffy, A preliminary study of the influence of experiential backgrounds of respondents to a reference survey for verification of FSV, in: 2016 IEEE International Symposium on Electromagnetic Compatibility (EMC), 2016, pp. 571–575.

[21] M.R. Johnson, FSV versus human subjective data evaluation; an informal survey, in: 2012 IEEE International Symposium on Electromagnetic Compatibility, 2012, pp. 679–684.

[22] IEEE Standard for Validation of Computational Electromagnetics Computer Modeling and Simulations, IEEE Std 1597.1-2008, 2008, pp. c1–41.

[23] IEEE Recommended Practice for Validation of Computational Electromagnetics Computer Modeling and Simulations, IEEE Std 1597.2-2010, 2011, pp. 1–124.

[24] A.P. Duffy, A.J.M. Martin, A. Orlandi, G. Antonini, T.M. Benson, M.S. Woolfson, Feature selective validation (FSV) for validation of computational electromagnetics (CEM). part I-the FSV method, IEEE Trans. Electromagn. Compat. 48 (3) (2006) 449–459.

[25] Q. Wang, Z. Jing, LRCS model verification based on the feature selective validation method, Opt. Laser Technol. 115 (2019) 384–389.

[26] G. Zhang, A.P. Duffy, H. Sasse, L.X. Wang, The use of probability density functions to improve the interpretation of FSV results, in: 2012 EEE International Symposium on Electromagnetic Compatibility, 2012, pp. 675–679.

[27] A.J.M. Martin, Quantitative data validation Ph. D. dissertation, De Montfort Univ., Leicester, U.K., 1999.

[28] D.E. Coleby, A.P. Duffy, A visual interpretation rating scale for validation of numerical models, Compel-the Int. J. Comput. Math. Electr. Electron. Eng. 24 (4) (2005) 1078–1092.

[29] R. Jauregui, G. Zhang, J. Rojas-Mora, O. Ventosa, F. Silva, A. Duffy, H. Sasse, Analysing transient phenomena in the time domain using the feature selective validation method, IEEE Trans. Electromagn. Compat. 56 (4) (2014) 825–834.

[30] R. Jauregui, P.J. Riu, F. Silva, Transient FDTD simulation validation, in: in Electromagnetic Compatibility (EMC) 2010 IEEE International Symposium on, 2010, pp. 257–262.

[31] R. Jauregui, J. Rojas-Mora, F. Silva, Study of transient phenomena with Feature Selective Validation Method, in: Progress in Electromagnetics Research Symposium (PIERS), 2011, pp. 2–6.

[32] A. Orlandi, A.P. Duffy, B. Archambeault, G. Antonini, D.E. Coleby, S. Connor, Feature selective validation (FSV) for validation of computational electromagnetics (CEM). Part II-assessment of FSV performance, Electromagn. Compat., IEEE Trans. 48 (3) (2006) 460–467.